J. Fluid Mech. (1995), *vol.* 290, *pp.* 279–298

The flow induced by the torsional oscillations of an elliptic cylinder

By N. RILEY AND M. F. WYBROW
School of Mathematics, University of East Anglia, Norwich NR4 7TJ, UK

(Received 22 July 1994 and in revised form 14 November 1994)

We consider the fluid motion induced when an elliptic cylinder performs small-amplitude torsional oscillations about an axis parallel to a generator which passes through either the centre or a point on the major or minor axis of the ellipse. In common with other fluid flows dominated by oscillatory motion, a time-independent, or steady streaming flow develops. This steady streaming exhibits several unusual and unexpected features, which are confirmed by experiment.

1. Introduction

In this paper we are concerned with the flow induced by the small-amplitude, torsional oscillations of a cylinder with elliptic cross-section in a viscous fluid that is otherwise at rest. The axis of oscillation, parallel to the cylinder generators, is placed at either the centre of the ellipse or at a point along its major or minor axis. Particular interest is focused upon the acoustic streaming, or time-averaged flow, that is induced by such a motion of the cylinder. Several novel, and unexpected, features associated with the steady streaming are predicted, and visualized in a simple experiment.

Steady streaming motions induced by vibrating objects in a fluid otherwise at rest, for which a generic term is acoustic streaming, have been observed, and studied, for more than a century. Overviews of the subject may be found in Riley (1967), who also reviews earlier work, and Lighthill (1978). A prototype problem is the circular cylinder that performs translational oscillations perpendicular to its generators. Two parameters characterize the flow: the dimensionless amplitude of the oscillation, and the so-called streaming Reynolds number which is based upon the magnitude of the induced steady streaming velocity. As Lighthill remarks, all worthwhile streaming motions are at high values of this Reynolds number, and it is the high-Reynolds-number regime with which we are concerned. Riley (1965), Stuart (1966) and Davidson and Riley (1972) have all studied the boundary layer on a circular cylinder performing translational vibrations. This has a double structure, namely an inner Stokes, or shear-wave, layer in which the steady streaming is generated, and an outer steady streaming boundary layer driven from the Stokes layer. The outer boundary layers collide to form jets along the axis of oscillation. Davidson & Riley also consider the streaming motion when an elliptic cylinder performs translational oscillations parallel to either the major or minor axis. Again jets are predicted to emerge along the axis of oscillation, and these have been observed and measured experimentally by Davidson & Riley. A different type of oscillatory motion, namely orbital flow, has the axis of oscillation moving in a small circle but with the orientation of the cylinder fixed. Longuet-Higgins (1970) and Riley (1971) have considered such orbital motion of a circular cylinder. A steady streaming is again induced in the Stokes layer, now with circulation about the cylinder, and this matches directly to an outer potential vortex flow. However, for orbital

motion of an elliptic cylinder Riley (1978) has shown that a second, outer boundary layer is again required before a match with the potential vortex can be satisfactorily made.

In this paper we consider the torsional, or angular, oscillations of an ellipse about an axis parallel to its generators, initially at its centre. For the limiting case of a circular cylinder there is no steady streaming, and we simply have a viscous shear wave propagating radially from the cylinder. For the other limiting case of a finite flat plate, vortices of alternate sign will be shed from each edge, and we may expect these to propagate as vortex pairs away from the plate on what is essentially the major axis. For an elliptic cylinder such a net flow away from it along the direction of the major axis would again be anticipated if the oscillation amplitude were sufficiently large to induce separation. However, for small-amplitude vibrations, when no flow separation takes place, we have the unexpected result that jets issue symmetrically from the cylinder surface, following a boundary-layer collision, along the direction of the minor axis. The boundary layer at the cylinder surface is again of double-structured type. If the axis of oscillation, or pivot, is now moved along the major axis of the ellipse a situation arises in which the steady streaming is directed, asymmetrically, along the direction of the semi-major axis where the pivot is placed. This is consistent with the asymmetric steady streaming analysed by Riley & Watson (1993) for the eccentric oscillations of a circular cylinder. As the pivot moves further out on the major axis we eventually recover the original situation, with jets forming along the minor axis, for now the cylinder is essentially performing translational vibrations along that axis. If the pivot is, instead, moved from the centre along the minor axis a quite different, and equally unexpected, sequence of events takes place. The jet from the end of the semi-minor axis on which the pivot is now placed bifurcates; the other one gradually weakens. As the pivot moves further out the bifurcated jets continue to separate, the other to weaken, until they lie along the major axis of the ellipse. With the pivot at large distances, this is consistent with the ellipse performing translational vibrations along the direction of the major axis.

The relative simplicity of the configuration, together with the unusual and unexpected streaming motions predicted, have prompted the construction of an experiment. This is described in the last section, and we remark here that our observations, by appropriate flow visualization techniques, confirm the unusual steady streaming flows we have described above.

2. Governing equations

We are concerned with the flow induced by a cylinder, of elliptical cross-section, that performs torsional oscillations about an axis, parallel to its generators, with angular velocity

$$\boldsymbol{\Omega} = \Omega_0 \cos \omega t' \boldsymbol{k}. \tag{2.1}$$

In (2.1) t' is time, $\boldsymbol{k}$ the unit vector parallel to a generator, and Ω_0, ω are constants. If a typical length is d, so that a typical velocity is $\Omega_0 d$, and t_0 is a typical time, where d and t_0 are to be chosen, the dimensionless unsteady Navier–Stokes equations may be written, in a frame of reference fixed to the cylinder, as

$$\frac{\partial}{\partial t}(\nabla^2\psi) + 2\delta \sin(\omega t_0 t) - \frac{\epsilon\delta}{h^2}\frac{\partial(\psi, \nabla^2\psi)}{\partial(u, v)} = \frac{\epsilon^2}{R_s}\nabla^4\psi, \tag{2.2}$$

where

$$\nabla^2\psi = \frac{1}{h^2}\left(\frac{\partial^2\psi}{\partial u^2} + \frac{\partial^2\psi}{\partial v^2}\right). \tag{2.3}$$

In these equations (u, v) are elliptic coordinates, related to rectangular coordinates in the (x, y) plane by

$$x = 2\,\mathrm{e}^{-u_0}\cosh u\cos v, \quad y = 2\,\mathrm{e}^{-u_0}\sinh u\sin v, \tag{2.4}$$

with $u \geqslant 0$, $0 \leqslant v \leqslant 2\pi$. The scale factor h is given by

$$h(u, v) = 2\,\mathrm{e}^{-u_0}(\sinh^2 u + \sin^2 v)^{1/2}, \tag{2.5}$$

and the stream function ψ determines the velocity components in the (u, v)-directions, respectively, as

$$v_u = \frac{1}{h}\frac{\partial \psi}{\partial v}, \quad v_v = -\frac{1}{h}\frac{\partial \psi}{\partial u}. \tag{2.6}$$

The no-slip condition is to be applied at the cylinder surface which we take as $u = u_0$. With this choice we note that if a, b are respectively the semi-major and -minor axes of our elliptic cylinder then our typical length d is given by $d = \frac{1}{2}a\,\mathrm{e}^{u_0}/\cosh u_0$, with $b/a = \tanh u_0$. As $u_0 \to 0, \infty$ the elliptic cylinder degenerates to either a flat plate or circular cylinder.

In (2.2) the three dimensionless parameters δ, ϵ and R_s are defined as

$$\delta = \omega t_0, \quad \epsilon = \Omega_0/\omega, \quad R_s = \Omega_0^2 d^2/\omega^2 \nu t_0, \tag{2.7}$$

where ν is the kinematic viscosity. Although it appears that three independent parameters characterize our flow, the obvious choice of ω^{-1} or Ω_0^{-1} for t_0 shows that, in fact, there are only two such characterizing parameters. In particular, we note that $\epsilon \ll 1$ is the situation with which we are most concerned throughout.

3. Initial flow development

In this section we consider the initial development of the flow when the oscillatory motion is initiated at $t = 0$, according to (2.1). We are particularly concerned with the manner in which the Stokes layer, that is initially formed at the surface of the cylinder, develops and breaks down in the high-frequency, high-Reynolds-number limit. This breakdown we interpret as a form of separation, or eruption, of fluid from the surface. We consider only the case of symmetric flow, when the axis of oscillation passes through the centre of the ellipse, since we believe there are no substantially new features to be uncovered in the asymmetric cases.

The obvious choice for the timescale t_0 is now Ω_0^{-1} so that, from (2.7),

$$\delta = \epsilon^{-1}, \quad R_s = \Omega_0^3 d^2/\omega^2 \nu. \tag{3.1}$$

From (3.1) we note that in (2.2) the quantity $Re = R_s/\epsilon^2 = \Omega_0 d^2/\nu$ plays the role of a conventional Reynolds number. We are concerned with the case $Re \gg 1$. In that case, and with $\epsilon \ll 1$, the leading term of (2.2), $\psi_0(u, v, t)$ say, satisfies

$$\frac{\partial}{\partial t}(\nabla^2 \psi_0) = -\frac{2}{\epsilon}\sin(t/\epsilon). \tag{3.2}$$

The solution of (3.2), with $\psi_0 = 0$ on $u = u_0$, and for which $\psi_0 \sim \mathrm{e}^{-2u_0}(\cosh 2u + \cos 2v)\cos(t/\epsilon)$ as $u \to \infty$, is

$$\psi_0 = \mathrm{e}^{-2u_0}\{\cosh 2u - \cosh 2u_0 + \cos 2v - \mathrm{e}^{-2(u-u_0)}\cos 2v\}\cos(t/\epsilon). \tag{3.3}$$

This does not satisfy the condition of no-slip at the surface $u = u_0$. The slip velocity V_s is given by

$$V_s(v, t) = -\frac{1}{h}\frac{\partial \psi_0}{\partial u}\bigg|_{u=u_0} = -\frac{\mathrm{e}^{-u_0}(\sinh 2u_0 + \cos 2v)}{(\sinh^2 u_0 + \sin^2 v)^{1/2}}\cos(t/\epsilon), \tag{3.4}$$

and this velocity of slip must be corrected through a boundary layer of thickness $O(Re^{-1/2})$, which we now consider.

First note that the vorticity vector ζ is given by $\zeta = (0, 0, \zeta) = (0, 0, -\nabla^2\psi)$. We now introduce new variables, denoted by an overbar, that acknowledge the boundary-layer scale, as

$$\bar{\psi} = Re^{1/2}\psi, \quad \bar{\zeta} = Re^{-1/2}\zeta, \quad \bar{u} = Re^{1/2}h_0(v)(u-u_0) \tag{3.5}$$

where $h_0(v) = h(u_0, v)$, so that (2.2) becomes

$$\frac{\partial\bar{\zeta}}{\partial t} + \frac{v_v}{h_0}\frac{\partial\bar{\zeta}}{\partial v} + \bar{v}_u\frac{\partial\bar{\zeta}}{\partial\bar{u}} = \frac{\partial^2\bar{\zeta}}{\partial\bar{u}^2}, \tag{3.6a}$$

with

$$\partial^2\bar{\psi}/\partial\bar{u}^2 = -\bar{\zeta}, \tag{3.6b}$$

and where

$$\bar{v}_u = \frac{1}{h_0}\frac{\partial\bar{\psi}}{\partial v}, \quad v_v = -\frac{\partial\bar{\psi}}{\partial\bar{u}}. \tag{3.6c}$$

In deriving (3.6) the additional assumption $\epsilon Re^{1/2} \gg 1$ has been made. This streamfunction–vorticity formulation of the boundary-layer equations has previously been exploited by Vasantha & Riley (1988), and Riley & Vasantha (1989). Its advantage is associated with the fact that the solution is periodic, period 2π, in v. The numerical scheme we have used is described in detail by those authors, and not repeated here. All our calculations have been carried out for an ellipse with $b/a = 0.5$, which corresponds to $u_0 = 0.549306$. In the calculations we have set the edge of the boundary layer at $\bar{u}_\infty = 80$, with mesh size $\delta t = \epsilon\pi/50$, $\delta v = \pi/100$ and $\delta\bar{u} = 0.1$. Numerical experimentation, and the experience of Vasantha & Riley (1988), shows that this mesh provides adequate resolution, and all results we display are accurate to the number of significant figures shown.

It is now well established that the failure of the unsteady boundary-layer equations, made manifest by the development of singular behaviour in the solution, heralds the onset of breakaway of fluid from the surface. Diverse examples are provided by the work of Banks & Zaturska (1979), Van Dommelen & Shen (1980) and Brown & Simpson (1982). In all these cases, the solution develops a singularity at a finite time. In the present case, for $\epsilon \ll 1$, we envisage that the $O(\epsilon)$ time-averaged secondary flow will result in an accumulation of fluid at some point on the surface of the ellipse from which there is an eruption at a finite time. This we suppose by analogy with the eruption of fluid from a circular cylinder which performs small-amplitude translational vibrations, Vasantha & Riley (1988). Such an eruption we expect, again by analogy, will result in jet-like flows, and this possibility is examined further in the next section. An obvious measure of the onset of failure, by flow separation or eruption, is the viscous displacement velocity defined by

$$v_d = \frac{1}{h_0}\frac{\partial}{\partial v}\int_0^{\bar{u}_\infty}(V_s - v_v)\,\mathrm{d}\bar{u}, \tag{3.7}$$

and we have monitored the maximum value of this, in $0 < v \leqslant 2\pi$, in our calculations. Vasantha & Riley (1988) found that the singular behaviour of v_d as $t \to t_s$, the eruption time, exhibits the behaviour $(t-t_s)^{-7/4}$, as in the work of Van Dommelen & Shen (1980). The breakdown that we have encountered is also consistent with this behaviour.

For $\epsilon \ll 1$, as already remarked, we expect a situation in which drift velocities of $O(\epsilon)$ result in an accumulation of fluid at a point from which the flow erupts, as on a circular cylinder that performs translational vibrations. However for $\epsilon \gg 1$ we may expect

ϵ	t_s	$\lvert\frac{1}{2}\pi - v_s\rvert$
10^3	0.54	1.414
0.2	1.9	0.660
0.1	21.0	0.408
0.05	29.0	0.314

TABLE 1. The main features of the solutions

separation of a more conventional type to occur in the regions of highest curvature. For intermediate values these mechanisms will compete. We set out the main features of our solutions in table 1. There t_s, v_s denote the time and location of the breakdown of the solution as determined from $(v_d)_{max}$ in (3.7).

We remark that for the largest value of ϵ we have, in fact, taken $\delta t = 0.0025$. There are several points to note. For the largest value of ϵ we are essentially considering an ellipse set into uniform rotation, with conventional flow separation taking place close to maximum curvature. As the amplitude of oscillation ϵ decreases this form of flow breakaway gives way to the second type of eruption due to accumulation of fluid as discussed. Of course the asymmetric thickening of the boundary layer about the major axis, close to maximum curvature, still influences the nature of the solution and in particular the point of breakaway. We may conjecture that for $\epsilon \ll 1$ this effect diminishes, and $v_s \to \frac{1}{2}\pi$ as $\epsilon \to 0$. To extend the results of table 1 to smaller values of ϵ is not easy. The breakdown time t_s increases: an estimate by Riley & Vasantha (1989) for oscillatory flow at a stagnation point gives $t_s = O(\epsilon^{-1})$, as ϵ decreases. And with $\delta t = O(\epsilon)$ the computational effort increases by a factor $O(\epsilon^{-2})$. Navier–Stokes calculations for this case have been carried out by S. C. R. Dennis (private communication). For $\epsilon = \pi^{-1}$ and $Re = O(10^3)$ the breakaway points of the flow from the cylinder are not, as here, symmetrically placed. However, as t increases, the flow in the neighbourhood of the cylinder develops into a quasi-periodic flow, symmetric about the minor axis of the ellipse along which jet-like structures emerge. We consider this quasi-periodic solution in the next section when $\epsilon \ll 1$.

4. Quasi-periodic flow

For this quasi-periodic flow ω^{-1} is a natural choice for the timescale t_0. As a consequence, in (2.2) we have $\delta \equiv 1$. Also note that $R_s = \Omega_0^2 d^2/\omega\nu = \epsilon Re$; the significance of this parameter, assumed to be $O(1)$, will emerge later. In this flow regime we are concerned with both the symmetric situation of §3 in which the axis of oscillation lies along the centre of the ellipse, and the asymmetric cases when the axis lies at some arbitrary point on either the major or minor axis. It proves convenient to develop the symmetric case first, in some detail and then outline more briefly the necessary modifications for the asymmetric cases.

4.1. *Symmetric flow*

Equation (2.2), with $\delta \equiv 1$, is to be solved subject to

$$\psi = \partial\psi/\partial u = 0 \quad \text{at} \quad u = u_0, \tag{4.1a}$$

$$\psi \sim e^{-2u_0}(\cosh 2u + \cos 2v)\cos t \quad \text{as} \quad u \to \infty. \tag{4.1b}$$

As is common with problems of this type we expand the streamfunction as

$$\psi(u,v,t) = \psi_0(u,v,t) + \epsilon\{\psi_1^{(u)}(u,v,t) + \psi_1^{(s)}(u,v)\} + \epsilon^2\psi_2(u,v,t) + \epsilon^3\psi_3(u,v,t) + O(\epsilon^4). \tag{4.2}$$

In (4.2) we have acknowledged the fact that the solution will not be purely periodic, but will have a non-zero time average, by splitting ψ_1 into a time-dependent or unsteady (u) part, and a time-independent or steady (s) part. Substituting (4.2) into (2.2) gives, at leading order,

$$\partial(\nabla^2\psi_0)/\partial t = -2\sin t.$$

The solution which satisfies the first of (4.1a), and (4.1b), is

$$\psi_0 = \mathrm{e}^{-2u_0}(\cosh 2u - \cosh 2u_0 + \cos 2v - \mathrm{e}^{-2(u-u_0)}\cos 2v)\cos t, \tag{4.3}$$

which is, of course, simply (3.3) on this new timescale. The no-slip condition is violated at $u = u_0$ where the slip velocity is given, as in (3.4), by

$$V_s(v,t) = -\frac{\mathrm{e}^{-u_0}(\sinh 2u_0 + \cos 2v)}{(\sinh^2 u_0 + \sin^2 v)^{1/2}}\mathrm{e}^{\mathrm{i}t} = -\bar{V}(v)\,\mathrm{e}^{\mathrm{i}t}. \tag{4.4}$$

Where complex notation is adopted, as in (4.4) and below, the real part is to be understood.

To satisfy the no-slip condition an inner boundary layer, the Stokes or shear-wave layer, has to be introduced. This is known to have thickness $O(\nu/\omega)^{1/2}$ which leads us to the inner variables

$$\Psi = \frac{R_s^{1/2}}{\sqrt{2\epsilon}}\psi, \quad \rho = \frac{h_0 R_s^{1/2}(u-u_0)}{\sqrt{2\epsilon}}. \tag{4.5}$$

As in the outer region we expand the streamfunction Ψ as

$$\Psi(\rho,v,t) = \Psi_0(\rho,v,t) + \epsilon\{\Psi_1^{(u)}(\rho,v,t) + \Psi_1^{(s)}(\rho,v)\} + O(\epsilon^2), \tag{4.6}$$

where we have again anticipated the presence of a time-independent part at $O(\epsilon)$. Substituting (4.5), (4.6) into (2.2) gives, at leading order,

$$\frac{\partial}{\partial t}\left(\frac{\partial^2\Psi_0}{\partial\rho^2}\right) = \frac{1}{2}\left(\frac{\partial^4\Psi_0}{\partial\rho^4}\right), \tag{4.7a}$$

with

$$\Psi_0 = \partial\Psi_0/\partial\rho = 0 \quad \text{at} \quad \rho = 0, \tag{4.7b}$$

$$\partial\Psi_0/\partial\rho \to \bar{V}\mathrm{e}^{\mathrm{i}t} \quad \text{as} \quad \rho\to\infty, \tag{4.7c}$$

where $\bar{V}$ is defined by (4.4). The solution of (4.7) is

$$\Psi_0 = \bar{V}(v)[\rho - \tfrac{1}{2}(1-\mathrm{i})\{1-\mathrm{e}^{-(1+\mathrm{i})\rho}\}]\mathrm{e}^{\mathrm{i}t}. \tag{4.8}$$

We consider next the terms of $O(\epsilon)$ in (4.6). Our particular concern is with the steady streaming at $O(\epsilon)$, represented by $\Psi_1^{(s)}$ in (4.6). Upon substitution of (4.6), with (4.5), into (2.2), and taking a time average, we have at $O(\epsilon)$,

$$\frac{\partial^2\Psi_1^{(s)}}{\partial\rho^4} = \frac{2}{h_0}\left(\frac{\partial\Psi_0}{\partial v}\frac{\partial^3\Psi_0}{\partial\rho^3} - \frac{\partial\Psi_0}{\partial\rho}\frac{\partial^3\Psi_0}{\partial\rho^2\,\partial v}\right)^{(s)}. \tag{4.9}$$

The superscript (s) on the right-hand side of (4.9) again indicates the time-independent part which results from time averaging. The solution of (4.9) for which

$$\Psi_1^{(s)} = \partial\Psi_1^{(s)}/\partial\rho = 0 \quad \text{at} \quad \rho = 0, \tag{4.10}$$

and for which $\partial \Psi_1^{(s)}/\partial\rho$ is bounded as $\rho \to \infty$, is

$$\Psi_1^{(s)} = \frac{2\bar{V}\dot{\bar{V}}}{h_0} g(\rho), \tag{4.11a}$$

where $$g(\rho) = 2\rho e^{-\rho}\sin\rho + 6e^{-\rho}\cos\rho + 4e^{-\rho}\sin\rho + \tfrac{1}{2}e^{-2\rho} + 3\rho - \tfrac{13}{2}, \tag{4.11b}$$

with $\bar{V}$ defined by (4.4), and a dot denotes differentiation with respect to v. It is well known, see for example Riley (1967), that vorticity created in this inner shear-wave layer, by the action of the Reynolds stresses on the right-hand side of (4.9), diffuses beyond it, and this leads to the boundedness condition on the velocity.

With Ψ_0, $\Psi_1^{(s)}$ determined we now take the outer expansion of the inner solution (4.6) which, written in outer variables, is

$$h_0 \bar{V}(u-u_0)e^{it} - \epsilon\frac{\bar{V}(1-i)}{\sqrt{2R_s^{1/2}}}e^{it} + 6\epsilon\bar{V}\dot{\bar{V}}(u-u_0) + S. \tag{4.12}$$

We note that the first term of (4.12) matches with ψ_0 in (4.3), and that the contribution S contains terms $O\{\epsilon(u-u_0)e^{it}\}$ which will match with the outer solution $\psi_1^{(u)}$, as we shall see, and terms $O(\epsilon^2 e^{2it})$. Both of these contributions to S feature in the outer expansion of $\Psi_1^{(u)}$ which we do not require explicitly.

We return now to the outer solution where our main aim is to derive information about the steady streaming, as represented by $\psi_1^{(s)}$ in (4.2). Introducing (4.2) into (2.2) we have, from the terms of $O(\epsilon)$,

$$\frac{\partial}{\partial t}(\nabla^2\psi_1^{(u)}) = \frac{1}{h^2}\frac{\partial(\psi_0, \nabla^2\psi_0)}{\partial(u,v)} \equiv 0, \tag{4.13}$$

since $\nabla^2\psi_0 = 2e^{it}$. We infer from (4.13) that

$$\nabla^2\psi_1^{(u)} = 0, \tag{4.14a}$$

with, from (4.12), $$\psi_1^{(u)} = -R_s^{-1/2}\bar{V}e^{i(t-\pi/4)} \quad \text{on} \quad u = u_0 \tag{4.14b}$$

and $$\psi_1^{(u)} \quad \text{bounded as} \quad u \to \infty. \tag{4.14c}$$

The solution of (4.14) for $\psi_1^{(u)}$ may be written as

$$\psi_1^{(u)} = R_s^{-1/2}\left(\tfrac{1}{2}a_0 + \sum_{n=1}^{\infty} a_n e^{-n(u-u_0)}\cos nv\right)e^{i(t-\pi/4)}, \tag{4.15a}$$

where $$a_n = -\frac{2}{\pi}\int_0^{\pi}\bar{V}\cos nv\,dv. \tag{4.15b}$$

The inner expansion of $\psi_1^{(u)}$ provides the matching condition for the term $O\{\epsilon(u-u_0)e^{it}\}$ of S in (4.12). Consider next the terms $O(\epsilon^2)$ in (2.2) which yield

$$\frac{\partial}{\partial t}(\nabla^2\psi_2) = \frac{1}{h^2}\frac{\partial(\psi_0, \nabla^2\psi_1^{(s)})}{\partial(u,v)}, \tag{4.16}$$

from which we deduce, using (4.3), that

$$\nabla^2\psi_2 = \frac{2e^{-2u_0}}{h^2}\Big\{(\sinh 2u + e^{-2(u-u_0)}\cos 2v)\frac{\partial}{\partial v}(\nabla^2\psi_1^{(s)}) + \sin 2v(1-e^{-2(u-u_0)})\frac{\partial}{\partial u}(\nabla^2\psi_1^{(s)})\Big\}\sin t + \phi_2(u,v), \tag{4.17}$$

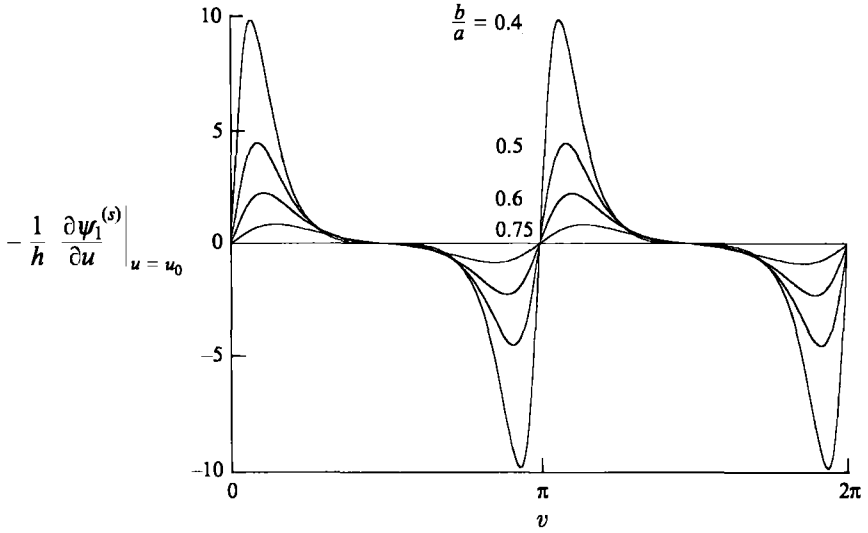

FIGURE 1. The velocity of slip at the edge of the shear-wave layer for various values of u_0, or b/a.

where both $\psi_1^{(s)}$ and ϕ_2 are unknown at this stage. Finally we consider the terms of $O(\epsilon^3)$ of (2.2), from which we have

$$\frac{1}{R_s}\nabla^4\psi_1^{(s)} + \frac{1}{h^2}\frac{\partial(\psi_1^{(s)}, \nabla^2\psi_1^{(s)})}{\partial(u,v)} = \frac{\partial}{\partial t}(\nabla^2\psi_3) - \frac{1}{h^2}\frac{\partial(\psi_0, \nabla^2\psi_2)}{\partial(u,v)}. \tag{4.18}$$

The left-hand side of (4.18) is independent of t, but both terms on the right-hand side are time dependent, the second by virtue of (4.3) and (4.17). As a consequence the equation satisfied by $\psi_1^{(s)}$ is

$$\frac{1}{R_s}\nabla^4\psi_1^{(s)} = \frac{1}{h^2}\left\{\frac{\partial\psi_1^{(s)}}{\partial v}\frac{\partial}{\partial u}(\nabla^2\psi_1^{(s)}) - \frac{\partial\psi_1^{(s)}}{\partial u}\frac{\partial}{\partial v}(\nabla^2\psi_1^{(s)})\right\}, \tag{4.19a}$$

with

$$\psi_1^{(s)} = 0, \quad \partial\psi_1^{(s)}/\partial u = 6\bar{V}\dot{\bar{V}} \quad \text{on} \quad u = u_0 \tag{4.19b}$$

from the matching condition (4.12), and

$$\partial\psi_1^{(s)}/\partial u \to 0 \quad \text{as} \quad u \to \infty. \tag{4.19c}$$

We see now that the steady streaming in the outer region is governed by the full Navier–Stokes equations in which the parameter R_s plays the role of the Reynolds number.

Before we discuss the solution of (4.19) we comment on the velocity of 'slip' $U^s = -\partial\psi_1^{(s)}/\partial u|_{u=u_0} = -6\bar{V}\dot{\bar{V}}$ that drives the steady streaming outside the shear layer. We present this quantity in figure 1 for various values of u_0, or b/a. This figure shows that the ends of the major axis, $v = 0, \pi$, are points of attachment of the outer flow from which it develops symmetrically up to the ends of the minor axis, $v = \frac{1}{2}\pi, \frac{3}{2}\pi$, where the velocity again is zero. These may be interpreted as stagnation points of separation. Our discussion of the initial flow development in §2 is consistent with this picture of the flow. Indeed we see how the Navier–Stokes calculations of S. C. R. Dennis (private communication) link our initial and quasi-periodic analyses. His numerical results show an initial breakaway of the flow close to, but not at, $v = \frac{1}{2}\pi, \frac{3}{2}\pi$ as do our

boundary-layer calculations for $\epsilon \ll 1$. In the subsequent flow development the flow becomes symmetrically disposed about the ellipse with jet-like structures emerging along the minor axis from $v = \frac{1}{2}\pi, \frac{3}{2}\pi$ for $Re \gg 1$. We concentrate now on solutions of (4.19) for which the streaming Reynolds number $R_s \gg 1$. As Lighthill (1978) has remarked it is only in this limit that worthwhile streaming motions are observed.

For $R_s \gg 1$ the outer steady streaming, determined from (4.19), is itself of a boundary-layer character. The thickness of this outer layer is $O(R_s^{-1/2})$, which we note is greater than that of the inner, shear-wave, layer by a factor $O(\epsilon^{-1})$. In this outer boundary layer we write

$$\psi_1^{(s)} = R_s^{-1/2}\tilde{\psi}_1^{(s)}, \quad u - u_0 = R_s^{-1/2}\tilde{u}.$$

When these variables are introduced into (4.19) and terms of relative order $R_s^{-1/2}$, and smaller, are ignored the resulting equation may be integrated once to give

$$\frac{\partial^3\tilde{\psi}_1^{(s)}}{\partial\tilde{u}^3} = \frac{\partial\tilde{\psi}_1^{(s)}}{\partial v}\frac{\partial^2\tilde{\psi}_1^{(s)}}{\partial\tilde{u}^2} - \frac{\partial\tilde{\psi}_1^{(s)}}{\partial\tilde{u}}\frac{\partial^2\tilde{\psi}_1^{(s)}}{\partial\tilde{u}\,\partial v} + \frac{\dot{h}_0}{h_0}\left(\frac{\partial\tilde{\psi}_1^{(s)}}{\partial\tilde{u}}\right)^2. \tag{4.20}$$

If, further, we write

$$\xi = v, \quad \eta = h_0\tilde{u}, \tag{4.21a}$$

and

$$u^s = -\frac{\partial\tilde{\psi}_1^{(s)}}{\partial\eta}, \quad v^s = \frac{1}{h_0}\frac{\partial\tilde{\psi}_1^{(s)}}{\partial\xi}, \tag{4.21b}$$

we recover the familiar two-dimensional boundary-layer equations for the outer steady streaming velocity (u^s, v^s), namely

$$\frac{u^s}{h_0}\frac{\partial u^s}{\partial\xi} + v^s\frac{\partial u^s}{\partial\eta} = \frac{\partial^2 u^s}{\partial\eta^2}, \tag{4.22a}$$

$$\frac{1}{h_0}\frac{\partial u^s}{\partial\xi} + \frac{\partial v^s}{\partial\eta} = 0, \tag{4.22b}$$

with

$$v^s = 0, \quad u^s = U^s = -6\frac{\bar{V}}{h_0}\frac{\mathrm{d}\bar{V}}{\mathrm{d}\xi} \quad \text{on} \quad \eta = 0, \quad u^s \to 0 \quad \text{as} \quad \eta \to \infty. \tag{4.22c}$$

We have integrated equations (4.22) in the direction of ξ increasing from the stagnation point of attachment $\xi = 0$ to $\xi = \frac{1}{2}\pi$. From symmetry considerations the solution at all other values of ξ is readily inferred. The numerical technique is a standard fully implicit finite-difference method, as described in detail by Davidson & Riley (1972). All derivatives are represented by central differences, and a quasi-linearization technique is employed. At each step in the ξ-direction the equations are solved iteratively until the non-linear system is satisfied within a prescribed tolerance. In implementing this procedure we have taken $\delta\xi = \pi/100$, $\delta\eta = 0.005$. As ξ increases, the boundary layer increases in thickness, and we have applied the outer boundary condition at $\eta = \eta_\infty$ where η_∞ increases, as v increases, in the range $10 \leqslant \eta_\infty \leqslant 20$. An important parameter is the momentum flux M in the boundary layer, defined as

$$M(\xi) = \int_0^\infty (u^s)^2\,\mathrm{d}\eta. \tag{4.23}$$

We see from figure 1 that as u_0, or b/a, decreases we expect M to increase, whilst as $u_0 \to \infty$, and the ellipse becomes near-circular, we shall find that $M \to 0$. We show, in

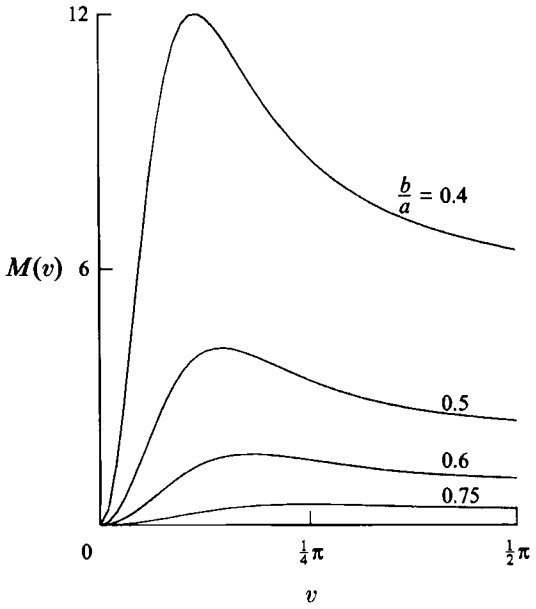

FIGURE 2. The momentum flux $M(v)$ in the outer boundary layer for various values of u_0, or b/a.

figure 2, the distribution of $M(\xi)$ for $0 \leqslant \xi \leqslant \frac{1}{2}\pi$ corresponding to the 'slip' velocities shown in figure 1. As anticipated $M(\xi)$ increases as u_0 decreases, in particular at $\xi = \frac{1}{2}\pi$. The boundary layer from $\xi = \pi$ develops in a similar manner, leading to an inevitable collision of these boundary layers at $\xi = \frac{1}{2}\pi$. The outcome of such a collision is a jet that emerges along the minor axis with, by symmetry, a similar jet emerging from $\xi = \frac{3}{2}\pi$. The strength of the jet, comparable to $M(\frac{1}{2}\pi)$, increases as u_0, or b/a, decreases. These jets are also a feature of the Navier–Stokes calculations of S. C. R. Dennis (private communication). This situation may be compared with that in which the elliptic cylinder performs translational vibrations, Davidson & Riley (1972). When the axis of oscillation is parallel to either the major or minor axis jets emerge, symmetrically, along the oscillation axis.

4.2. *Asymmetric flow*

In §4.1 above we have studied a flow with symmetry about both the major and minor axes of the ellipse when the axis of oscillation or pivot lies along the centre of the cylinder. We now consider the modifications to the flow when the pivot is placed on either the major or minor axis of the ellipse.

(i) *Pivot on major axis*

Suppose the pivot is located a distance $l = l'/d$ from the centre of the ellipse along $v = \pi$. Our governing equations are as before except that we now require

$$\psi \sim \{e^{-2u_0}(\cosh 2u + \cos 2v) + 2le^{-u_0}(\cosh u \cos v \cos\alpha + \sinh u \sin v \sin\alpha)\}e^{it}, \quad (4.24)$$

as $u \to \infty$, where α is the angular displacement of the ellipse. With $\alpha = \epsilon \sin t$ (4.24) may be written as

$$\psi \sim \{e^{-2u_0}(\cosh 2u + \cos 2v) + 2le^{-u_0}\cosh u \cos v\}e^{it} - i\epsilon l e^{-u_0}\sinh u \sin v\, e^{2it} + O(\epsilon^2). \quad (4.25)$$

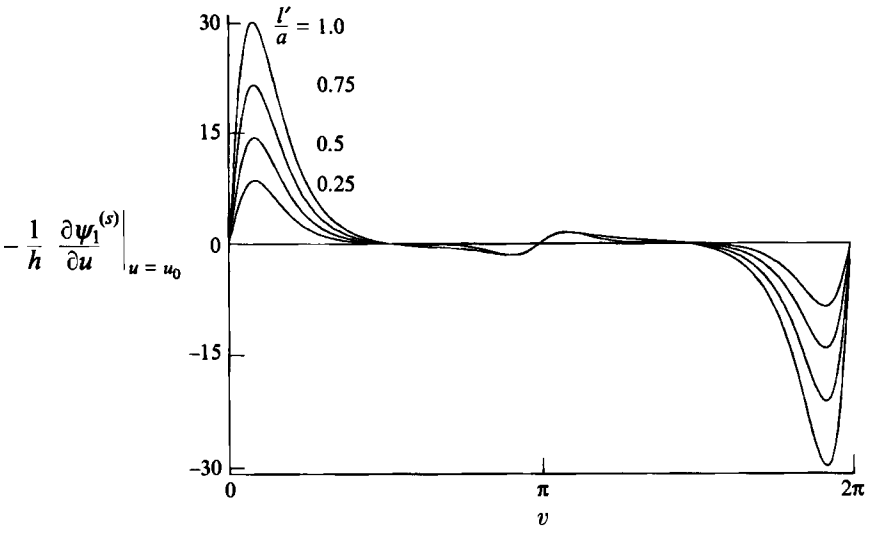

FIGURE 3. The velocity of slip at the edge of the shear-wave layer for an ellipse with $b/a = 0.5$ and the oscillation axis at various values, l'/a, along the semi-major axis $v = \pi$.

We again expand the outer solution ψ as in (4.2) where now the leading term, which behaves like the leading term of (4.25) rather than (4.1*b*) as $u \to \infty$, is

$$\psi_0 = [e^{-2u_0}\{\cosh 2u - \cosh 2u_0 + (1 - e^{-2(u-u_0)})\cos 2v\} + 2le^{-u_0}\cos v\{\cosh u - e^{-(u-u_0)}\cosh u_0\}]e^{it}.$$

The corresponding velocity of slip at $u = u_0$ gives

$$\bar{V}(v) = \{e^{-u_0}(\sinh 2u_0 + \cos 2v) + le^{u_0}\cos v\}(\sinh^2 u_0 + \sin^2 v)^{-1/2}. \tag{4.26}$$

The inner solution is also developed as in (4.6) and Ψ_0, $\Psi_1^{(s)}$ are as in (4.8), (4.11) with $\bar{V}$ given by (4.26). Returning to the outer solution at $O(\epsilon)$, and first to $\psi_1^{(u)}$, we see that there is a term as before, forced by the outflow from the Stokes layer, given by (4.15) with $\bar{V}$ as in (4.26). Call this original contribution $\psi_{10}^{(u)}$. There is an additional contribution say $\psi_{1a}^{(u)}$, at this order which satisfies, from (4.13),

$$\nabla^2\psi_{1a}^{(u)} = 0 \quad \text{with} \quad \psi_{1a}^{(u)} = 0 \quad \text{on} \quad u = u_0 \tag{4.27a}$$

and, from (4.25), as $u \to \infty$

$$\psi_{1a}^{(u)} \sim -ile^{-u_0}\sinh u \sin v e^{2it}. \tag{4.27b}$$

The solution of (4.27) for $\psi_{1a}^{(u)}$ is

$$\psi_{1a}^{(u)} = -ile^{-u_0}(\sinh u - e^{-(u-u_0)}\sinh u_0)\sin v e^{2it}, \tag{4.28}$$

and the complete time-dependent part of the solution at $O(\epsilon)$ is $\psi_1^{(u)} = \psi_{10}^{(u)} + \psi_{1a}^{(u)}$. At $O(\epsilon^2)$ we again have (4.16), from which $\nabla^2\psi_2$ is given by an expression of the form (4.17) where only the detail of the coefficient of the term $O(\sin t)$ changes. The subsequent arguments which lead to the problem for $\psi_1^{(s)}$ are unchanged. In particular, for $R_s \gg 1$, the problem for the outer steady streaming reduces to the solution of (4.22) where now $\bar{V}$ is given by (4.26).

The slip velocity U^s at the outer edge of the Stokes layer, which drives the outer steady streaming, is shown in figure 3. These results are for a single ellipse with $u_0 =$

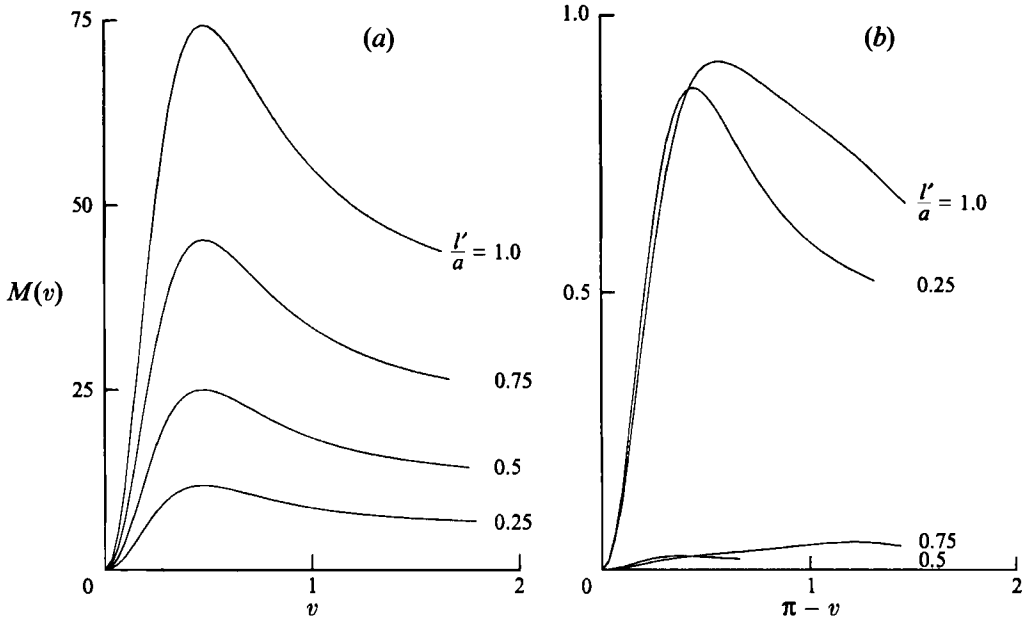

FIGURE 4. The momentum flux $M(v)$ in the outer boundary layer from (*a*) $v = 0$ and (*b*) $v = \pi$, for the slip velocities shown in figure 3.

0.5493 which corresponds to $b/a = 0.5$, and are plotted for various values of l'/a, up to the end of the major axis. We note that for these eccentric oscillations we can expect a much stronger flow to originate at the stagnation point of attachment $v = 0$ than at the corresponding point $v = \pi$. It is not immediately apparent from this figure, but in some cases U_s changes sign more than once in $0 \leqslant v \leqslant \pi$, but always in a region in which $|U_s| \ll 1$. We have integrated (4.22) numerically, as described in §4.1, from $v = 0$ in the direction of v increasing, and from $v = \pi$ in the direction of v decreasing. In each case we have terminated the calculation at the first point for which $U_s = 0$. The results for the momentum flux are shown, respectively, in figures 4(*a*) and (*b*). In all of the cases shown the momentum flux from the point of attachment $v = 0$ exceeds that from the point $v = \pi$ by a factor $O(10)$. We may infer, therefore, that the steady streaming from $v = 0$ overwhelms that from $v = \pi$ and that there is a net steady flow, superimposed on the basic fluctuating flow, along the direction of the semi-major axis $v = \pi$. This is consistent with the flow due to an eccentrically oscillating circular cylinder discussed by Riley & Watson (1993), and visualized experimentally by Taneda (1980). Of course, as the pivot moves out further along the major axis with $l' > a$ there will be yet another change in the character of the acoustic streaming, because, for $l' \gg a$, and with $\epsilon l \ll 1$, the situation will become one in which the cylinder is effectively performing *transverse* oscillations in the direction of its minor axis. In that case, as Davidson & Riley (1972) have demonstrated, the streaming manifests itself as jet-like flows along $v = \pm\frac{1}{2}\pi$.

In summary we have the following sequence of events, all of which exhibit symmetry about the major axis of the ellipse. For the case in which the pivot is at the centre of the ellipse the streaming manifests itself as jet-like flows emerging along the semi-minor axes $v = \pm\frac{1}{2}\pi$. As the pivot is moved along the major axis a point is reached, before $l' = a$, at which the streaming is predicted to be unidirectional along the semi-major axis $v = \pi$. But as the pivot is moved further in that direction the streaming finally reverts

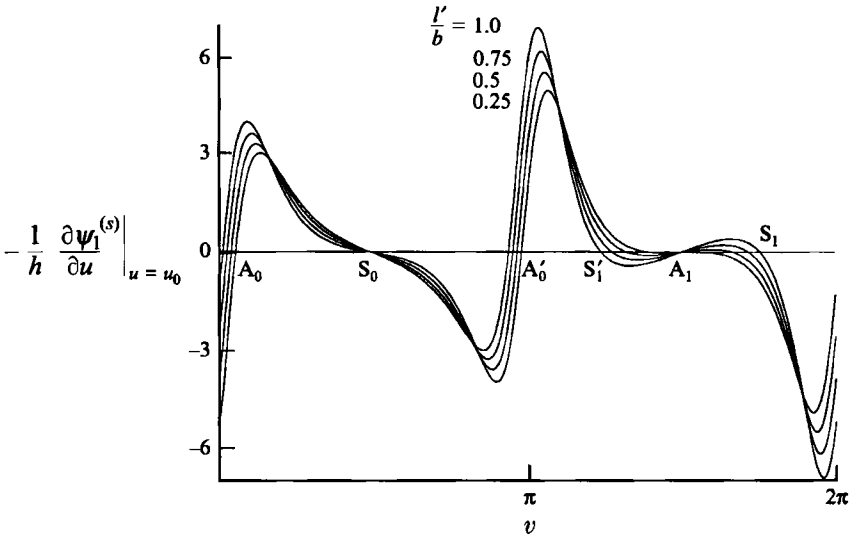

FIGURE 5. The velocity of slip at the edge of the shear-wave layer for an ellipse with $b/a = 0.5$ and the oscillation axis at various values, l'/b, along the semi-minor axis $v = \frac{3}{2}\pi$.

to its original configuration with streaming again along $v = \pm\frac{1}{2}\pi$. Such an unexpected sequence of events was unsuspected *a priori*.

(ii) *Pivot on minor axis*

We now consider the case when the pivot is located at a distance $l = l'/d$ from the centre of the ellipse along the semi-minor axis $v = \frac{3}{2}\pi$.

Our development of the solution closely mirrors that for case (i). In place of (4.24) we now require, as $u \to \infty$,

$$\psi \sim \{e^{-2u_0}(\cosh 2u + \cos 2v) + 2le^{-u_0}(\sinh u \sin v \cos\alpha - \cosh u \cos v \sin\alpha)\}e^{it}, \quad (4.29)$$

or, with $\alpha = \epsilon \sin t$,

$$\psi \sim \{e^{-2u_0}(\cosh 2u + \cos 2v) + 2le^{-u_0}\sinh u \sin v\}e^{it} + i\epsilon l e^{-u_0}\cosh u \cos v\, e^{2it} + O(\epsilon^2). \quad (4.30)$$

The leading term of the expansion (4.2) is now given by

$$\psi_0 = [e^{-2u_0}\{\cosh 2u - \cosh 2u_0 + (1 - e^{-2(u-u_0)})\cos 2v\} + 2le^{-u_0}\{(\sinh u - e^{-(u-u_0)}\sinh u_0)\sin v\}]e^{it}.$$

The corresponding velocity of slip at $u = u_0$ now gives

$$\bar{V}(v) = \{e^{-u_0}(\sinh 2u_0 + \cos 2v) + le^{u_0}\sin v\}(\sinh^2 u_0 + \sin^2 v)^{-1/2}. \quad (4.31)$$

For the inner solution Ψ_0 and $\Psi_1^{(s)}$ are again unchanged, except that now $\bar{V}$ is given by (4.31). For the outer solution at $O(\epsilon)$, $\psi_{10}^{(u)}$ is affected only by the change in $\bar{V}$ whilst $\psi_{1a}^{(u)}$ satisfies (4.27) but with the outer boundary condition replaced, from (4.30), by

$$\psi_{1a}^{(u)} \sim ile^{-u_0}\cosh u \cos v\, e^{2it} \quad \text{as} \quad u \to \infty,$$

so that

$$\psi_{1a}^{(u)} = ile^{-u_0}(\cosh u - e^{-(u-u_0)}\cosh u_0)\cos v\, e^{2it}. \quad (4.32)$$

The outer steady streaming, using exactly the same arguments as before, satisfies (4.19) or, in the high-Reynolds-number limit (4.22) with $\bar{V}$ defined in (4.31).

The slip velocity U^s at the outer edge of the Stokes layer that drives the outer streaming is shown in figure 5. The results shown are again for a single ellipse with

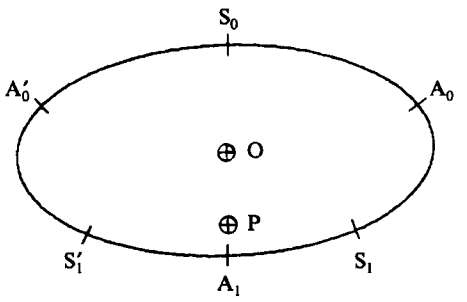

FIGURE 6. Points of attachment and separation on the ellipse.

$u_0 = 0.5493$ or $b/a = 0.5$, and are given for various values of l'/b up to the end of the minor axis.

Before we comment in detail on this case we note the following. As the pivot moves out along the minor axis, and beyond $l' = b$ to a sufficiently great distance, the motion of the cylinder is effectively that of transverse oscillations along the major axis. We know from Davidson & Riley (1972) that for such a situation the steady streaming is jet-like along the major axis. So, with the pivot at the centre the jets are directed along $v = \pm\frac{1}{2}\pi$, but for $l \gg 1$ we may expect them to be aligned along $v = 0, \pi$. We consider how this transformation takes place.

Consider the slip velocity U^s in figure 5, in relation to figure 6. There is symmetry, clearly, about the minor axis. The point S_0, which is a point of separation when the pivot point P is at the ellipse centre O remains a point of separation. The points A_0, A_0' will be stagnation points of attachment, originally at $v = 0, \pi$ when $l = 0$, with the arclength $A_0 S_0$ decreasing as l increases. At $v = \frac{3}{2}\pi$ we have a point of attachment A_1. This point, we recall, is a point of separation in the symmetric case, when O and P coincide, with a jet emerging from it. S_1, S_1' are points at which $U^s = 0$. These are not points of separation from which jets emerge, as we see from momentum flux arguments below, but such points will be close to them. Our prediction is, then, that the jet originally emerging from $v = \frac{3}{2}\pi$ when $l = 0$ bifurcates into two emergent jets, with a third jet originating at $v = \frac{1}{2}\pi$. As l increases, and the pivot point extends beyond the edge of the semi-minor axis $v = \frac{3}{2}\pi$, the points A_0, A_0' converge upon S_0 until that point is one of attachment; and S_1, S_1' move towards the ends of the major axis until we have the limiting situation with jets emerging along $v = 0, \pi$ as appropriate to what are then effectively transverse vibrations parallel to the major axis. To illustrate these features further we again consider the momentum flux in the boundary layers. First, in figure 7(*a*) we have the momentum flux as a function of v between attachment A_0 and S_0. As l'/b increases, so the sector $A_0 S_0$ decreases, as does the terminal momentum flux. This implies an ever-weakening jet emergent from S_0 as l'/b increases. Next, in figure 7(*b*) we show the momentum flux in the sector $A_0 S_1$. This increases as l'/b increases, as does the momentum flux along $A_1 S_1$ shown in figure 7(*c*). The latter increases more dramatically. As l'/b increases indefinitely the terminal momentum fluxes in sectors $A_0 S_1$ and $A_1 S_1$ will tend to the same value. In figures 7(*b*) and 7(*c*) we see an imbalance of momentum flux as the point S_1, at which $U^s = 0$, is approached. A consequence of this is that, just as in case (i), we may not expect the point of separation to be at S_1, but in this case to be displaced towards A_1. Only when l'/b is substantial may we anticipate the emergence of jets that are clearly distinguishable one from the other.

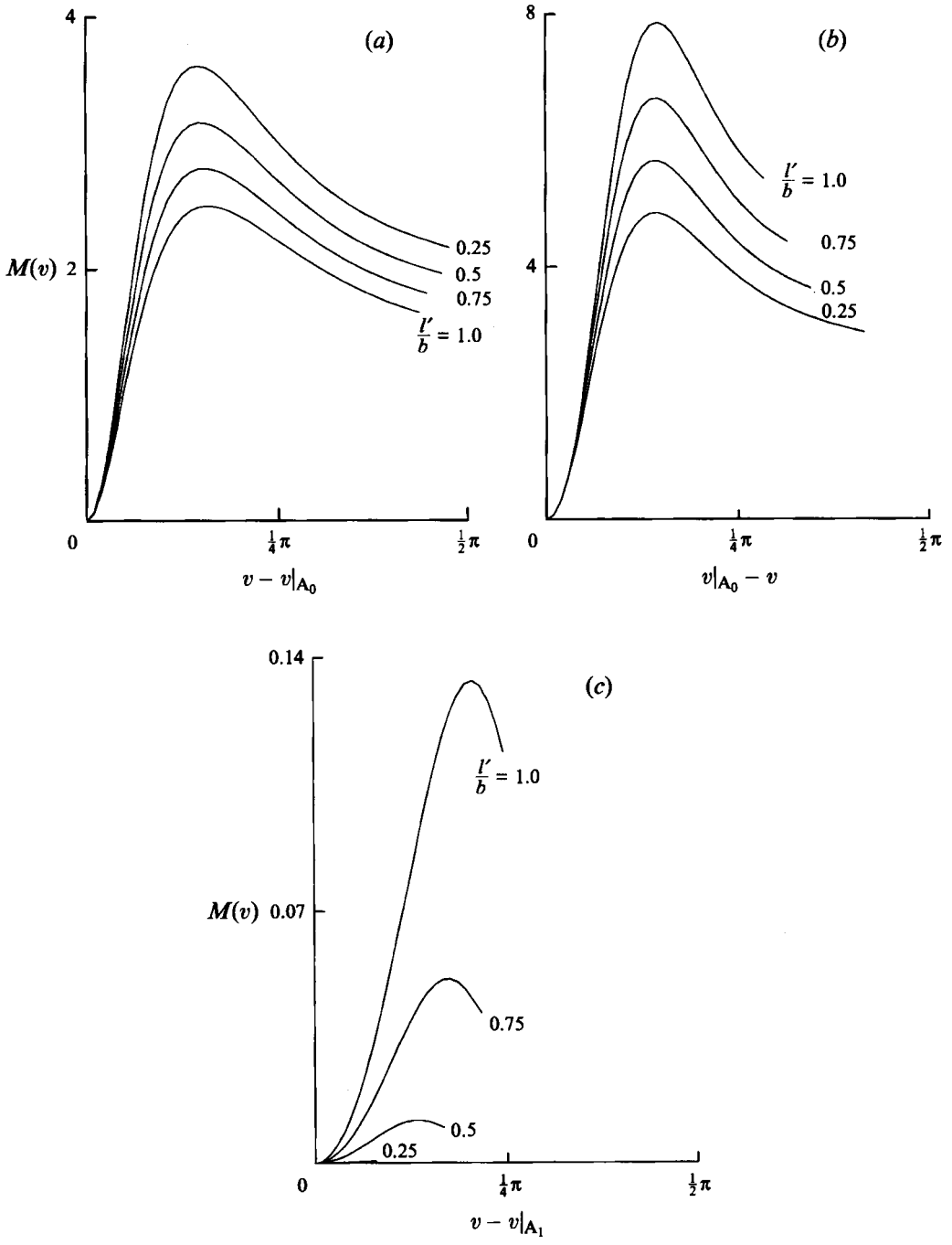

FIGURE 7. The momentum flux $M(v)$ in the outer boundary layer: (*a*) from A_0 to S_0; (*b*) from A_0 to S_1'; (*c*) from A_1 to S_1.

5. Experiments

The steady streaming flows we have discussed in §4 are both unexpected and varied. This fact has stimulated us to construct a simple experiment in order to verify the

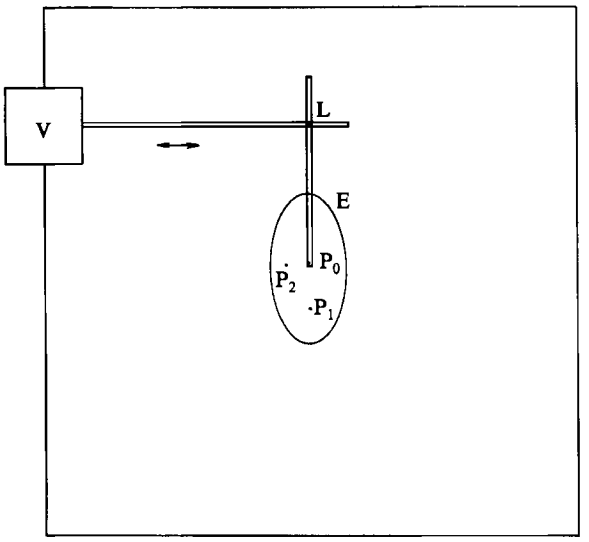

FIGURE 8. A schematic diagram of the experiment.

predictions we have made. This is shown in plan form in figure 8. The working fluid is water with kinematic viscosity $\nu = 0.01$ cm^2 s^{-1} at room temperature. It is contained in a rectangular tank constructed from Perspex acrylic of dimensions 30 cm in depth, and 45 cm × 45 cm in plan. A lid seals the tank and prevents any unwanted free-surface effects. Relief holes at each corner allow air bubbles, that form beneath the lid, to be withdrawn. The elliptic cylinder itself, E, is constructed from 'Delrin', measures 30 cm in length and 4 cm × 2 cm in cross-section, and is mounted vertically in the tank. Pivot points $P_i (i = 0, 1, 2)$ are located at the centre, and along the major and minor axes of the ellipse respectively. The upper pivot penetrates the lid, and to it is attached a horizontal arm. This in turn is attached, via a simple linkage L, to the horizontal arm of a small vibrator V clamped to the edge of the tank. For flow visualization purposes the fluid was seeded with 'Dantec' pearlescent material. Illumination was provided by two standard slide projectors, which were arranged to give a sheet of light of approximately 1 cm in thickness at the mid-plane. The amplitude and frequency of the vibrations could be varied. However, for the flows visualized in figure 9 these were fixed at an angular amplitude of $\epsilon = 0.25$ and frequency $\omega = 4$ Hz. The corresponding streaming Reynolds number $R_s = 352$. The visualized results shown in figure 9 were obtained with a Pentax ME Super 35 mm camera using Ilford FP4 film, mounted about 1 m above the tank. Exposure times were 1 s at f3.5 for figure 9(*a*) and 2 s at f4 for the remaining illustrations of figure 9.

Consider first figure 9(*a*). In this particular example the pivot is at position P_2 close to the end of the semi-minor axis, and we see the onset of a jet erupting from the end of that axis. This is typical of the onset of a jet flow, characterized by the appearance of a vortex pair, and was clearly observed in all the experiments with symmetry about the minor axis. Our analysis of §3 does not go beyond predicting the breakdown of the boundary-layer solution. Moreover, even when the quasi-periodic flow has symmetry about $v = \pm\frac{1}{2}\pi$ the breakdown predicted in §3 is not at these points, nor is it in the Navier–Stokes calculations of S. C. R. Dennis. However, we have not been able to detect, by eye, an eruption from the boundary layer, in these cases, other than at $v = \pm\frac{1}{2}\pi$. We may conclude that the breakdown, or separation, point moves very rapidly to give the symmetric eruption shown in figure 9(*a*). This is certainly consistent with

the Navier–Stokes calculations. In figure 9(*b*), where as in 9(*a*) the mean position of the ellipse is shown, the pivot is at the centre P_0 and the flow is symmetrical about both the major and minor axes. The flow within a few centimetres from the ellipse has evolved to its quasi-periodic state. The jet-like steady streaming has developed along the direction of the minor axis exactly as we have predicted. Entrainment into the jet, and also into the boundary layers at the ellipse that feed it, are clearly seen. The pivot for the example shown in figure 9(*c*) is now placed halfway along the semi-major axis $v = \pi$. The theoretical prediction from §4 indicates that a boundary layer develops from the stagnation point at $v = 0$ which is much stronger in terms of its momentum flux than the boundary layer originating from the stagnation point at $v = \pi$. The former may, therefore, be expected to overwhelm the latter following the inevitable collision between them. This is seen to be the case with the collision resulting in a separation from the surface of the jet-like flows from $v \approx \pm\frac{3}{4}\pi$, approximately parallel to the major axis. In this case the steady streaming flow is unstable and the net result is a broad, right to left in figure 9(*c*), net flow exactly as predicted. Again there is entrainment into the boundary layers at the ellipse. The initiation of the flow shown in figure 9(*c*) has features in common with figure 9(*a*). Now, however, as the boundary layers collide, and the flow erupts from the surface, each vortex pair is dominated by the stronger flow. The resulting structure, from each eruption point, has the appearance of a single vortex and these move out along lines $v \approx \pm\frac{3}{4}\pi$. The final configuration, shown in figure 9(*d*, *e*), has the pivot close to the end of the semi-minor axis, shown as P_2 in figure 8. In figure 9(*d*) we see a jet-like structure emerging from the stagnation point at the end of the semi-minor axis furthest from the pivot. This is similar to that shown in figure 9(*b*), where the pivot is centrally placed, as expected from the analysis of §4. Finally, in figure 9(*e*), the jet emerges from the stagnation point close to the pivot. Recall, from §4, that the jet emerging from this stagnation point in the case when the pivot is at P_0 bifurcates as the pivot is moved towards it along the semi-minor axis. Ultimately, we have argued, as the pivot moves off the ellipse in this direction the two parts of the bifurcated jet continue to separate until they are aligned with the major axis. In figure 9(*e*), see also figure 9(*a*), we see clearly the bifurcation of the jet. Since the two parts into which the jet has divided emerge in a direction towards the minor axis, as may be expected from the momentum fluxes in the boundary layers from which they are formed, they merge in this case into a single jet that moves out along the minor axis.

For the experiments described above ϵ and ω were not varied. However, our discussion in §3 shows that as the oscillation amplitude decreases the time of breakdown of the boundary-layer solution, from the onset of the flow, and hence the establishment of a quasi-periodic flow, increases. We have tested this in our experiment by varying ϵ with ω fixed at 4 Hz. The time t_s' at which the flow erupts from the boundary layer was estimated, by eye, from the first appearance of the vortex pair shown in figure 9(*a*). The results, which are for the pivot at P_0, are shown in table 2 where the streaming Reynolds number R_s is also shown. Although the results are not directly comparable with those in table 1, for which the parameter R_s is effectively infinite, the trend, as ϵ decreases, of t_s increasing, is evident.

We conclude that the experiments described in this section provide striking evidence in support of the theoretical predictions made in §4 for the unusual and unexpected time-averaged flows associated with the torsional oscillations of an ellipse.

The authors are indebted to Dr Chris Retzler of City University for help and advice on flow visualization. M.F.W. is indebted to SERC for support in the form of an earmarked studentship.

(*a*)

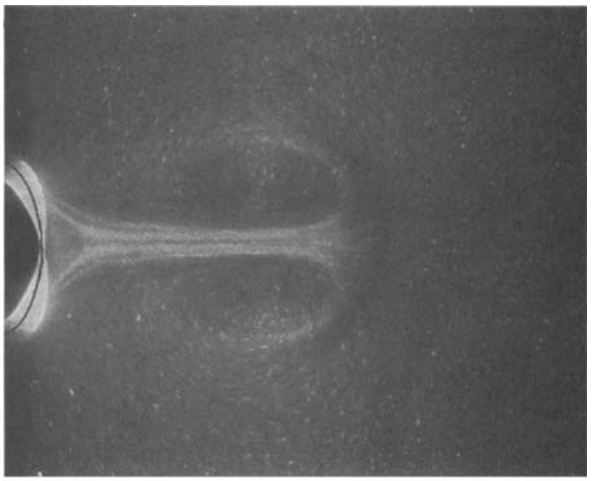

(*b*)

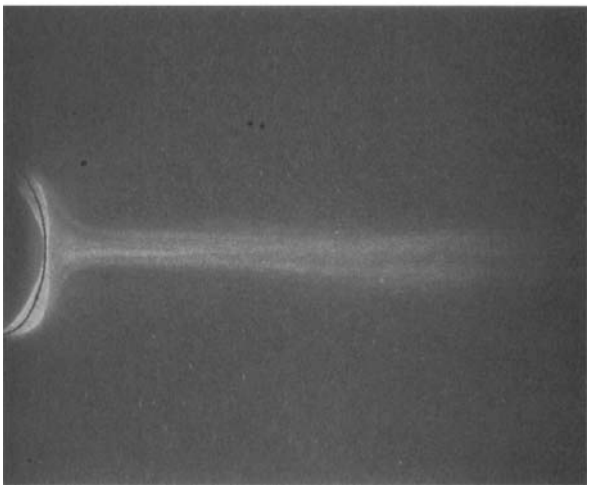

(*c*)

FIGURE 9(*a*–*c*). For caption see facing page.

(*d*)

(*e*)

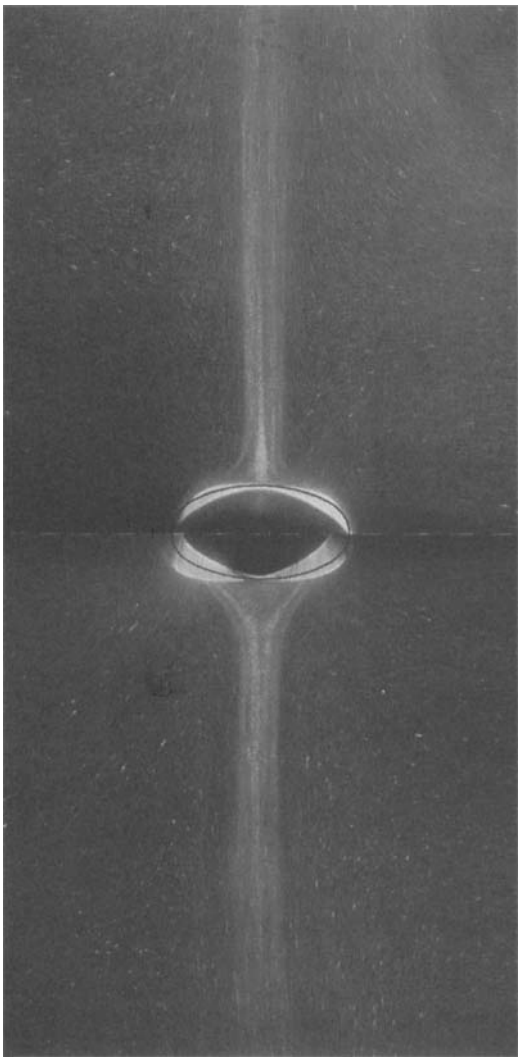

FIGURE 9. (*a*) An example of jet initiation; (*b*) The jet along the semi-minor axis with the pivot at P_0; (*c*) The steady streaming induced when the pivot is placed at P_1, halfway along the semi-major axis $v = \pi$; (*d*) The jet along the semi-minor axis $v = \frac{1}{2}\pi$ when the pivot is at P_2, close to the end of the semi-minor axis $v = \frac{3}{2}\pi$. (*e*) As (*d*) but showing the jet along the semi-minor axis $v = \frac{3}{2}\pi$.

ϵ	t'_s (s)	R_s
0.25	3.2	352
0.24	3.6	324
0.23	4.6	298
0.22	4.4	272
0.20	5.3	225
0.18	6.3	182
0.14	8.0	110
0.13	12.4	95

TABLE 2.

REFERENCES

BANKS, W. H. H. & ZATURSKA, M. B. 1979 The collision of unsteady laminar boundary layers. *J. Engng Maths* **13**, 193–212.

BROWN, S. N. & SIMPSON, C. J. 1982 Collision phenomena in free-convective flow over a sphere. *J. Fluid Mech.* **124**, 123–137.

DAVIDSON, B. J. & RILEY, N. 1972 Jets induced by oscillatory motion. *J. Fluid Mech.* **53**, 287–303.

LIGHTHILL, M. J. 1978 Acoustic streaming. *J. Sound Vib.* **61**, 391–418.

LONGUET-HIGGINS, M. S. 1970 Steady currents induced by oscillations round islands. *J. Fluid Mech.* **42**, 701–720.

RILEY, N. 1965 Oscillating viscous flows. *Mathematika* **12**, 161–175.

RILEY, N. 1967 Oscillatory viscous flows: review and extension. *J. Inst. Maths Applics.* **3**, 419–434.

RILEY, N. 1971 Stirring of a viscous fluid. *Z. Angew Math. Phys.* **22**, 645–653.

RILEY, N. 1978 Circular oscillations of a cylinder in a viscous fluid. *Z. Angew Math. Phys.* **29**, 439–449.

RILEY, N. & VASANTHA, R. 1989 An unsteady stagnation-point flow. *Q. J. Mech. Appl. Maths* **42**, 511–521.

RILEY, N. & WATSON, E. J. 1993 Eccentric oscillations of a circular cylinder in a viscous fluid. *Mathematika* **40**, 187–202.

STUART, J. T. 1966 Double boundary layers in oscillatory viscous flows. *J. Fluid Mech.* **24**, 673–687.

TANEDA, S. 1980 Visualization of steady flows induced by a circular cylinder performing a rotary oscillation about an eccentric axis. *J. Phys. Soc. Japan* **49**, 2038–2041.

VAN DOMMELEN, L. L. & SHEN, S. F. 1980 The spontaneous generation of the singularity in a separating laminar boundary layer. *J. Comput. Phys.* **38**, 125–140.

VASANTHA, R. & RILEY, N. 1988 On the initiation of jets in oscillatory viscous flows. *Proc. R. Soc. Lond.* A **419**, 363–378.